Chemical Engineering Science 134 (2015) 880–886

Contents lists available at ScienceDirect

Chemical Engineering Science

journal homepage: www.elsevier.com/locate/ces

Co-rotating twin-screw extruders: Detailed analysis of conveying elements based on smoothed particle hydrodynamics. Part 2: Mixing

Andreas Eitzlmayr [a], Johannes Khinast [a,b,*]

[a] Institute for Process and Particle Engineering, Graz University of Technology, Inffeldgasse 13, 8010 Graz, Austria
[b] Research Center Pharmaceutical Engineering, Inffeldgasse 13, 8010 Graz, Austria

HIGHLIGHTS

- We applied SPH to study mixing in a co-rotating twin-screw extruder.
- Various mixing mechanisms were distinguished.
- Mixing depends significantly on the actual operation state.
- Mixing rates are similar for completely and partially filled screw elements.
- Completely filled elements mix better due to the higher residence time.

ARTICLE INFO

Article history:
Received 5 November 2014
Received in revised form
15 April 2015
Accepted 18 May 2015
Available online 3 June 2015

Keywords:
Smoothed particle hydrodynamics
SPH
Co-rotating twin-screw extruder
Complex geometry
Partially filled
Mixing

ABSTRACT

A novel approach for the simulation of the flow in co-rotating twin-screw extruders based on smoothed particle hydrodynamics (SPH) was presented in Part 1. Specifically, we showed detailed results for the flow field in a completely filled conveying element, which are in excellent agreement with data from the literature obtained with computational fluid dynamics (CFD). Moreover, we studied the flow in the partially filled conveying element, facilitated by the inherent capabilities of SPH for modeling free-surface flows. In Part 2, we show a detailed analysis of the mixing effects based on the presented SPH simulations. We studied the mixing using tracer particles for the completely and partially filled states, evaluated the time evolution of the intensity of segregation and fitted kinetic laws in order to determine mixing rates. We conducted this separately for overall mixing and axial mixing and analyzed the contributions of axial and cross mixing to the overall mixing rates. We showed these results for various operation states and finally, presented a case study highlighting the effect of the residence time on mixing together with the determined mixing rates per screw revolution. This confirms that SPH is a very promising tool for the investigation of mixing in complex geometries in both, completely filled and partially filled states. The presented results provide an excellent basis for the further improvement of simplified models of entire extrusion processes, including a quantification of mixing.

1. Introduction

In Part 1 (Eitzlmayr and Khinast, 2015), we presented the use of the smoothed particle hydrodynamics method (SPH, e.g., (Monaghan, 1994, 2000, 2005)) for the simulation of the flow in co-rotating twin-screw extruders, which are widely used in different industries and increasingly attract interest in the pharmaceutical manufacturing (see, e.g., Breitenbach, 2002; Ghebre-Sellassie and Martin, 2003; Kleinebudde, 2011; Douroumis, 2012; Repka et al., 2013). We presented detailed results for the Newtonian, isothermal flow in a completely filled conveying element with variable backpressure, which was also studied by Bierdel (2008) using the finite volume method (FVM). We obtained excellent agreement with these data for the flow rate and the power input. Even more, we presented data for the flow in the partially filled conveying element with variable filling ratio. Since the simulation of partially filled extruders is problematic with well-established, mesh-based computational fluid dynamics methods (CFD), comparable data are rare for this case. However, the trends of our results are in agreement with data shown by Pokriefke

Abbreviations: 1D, one-dimensional; FVM, finite volume method; SMEC, specific mechanical energy consumption; SPH, smoothed particle hydrodynamics; STL, surface tessellation language

* Corresponding author at: Institute for Process and Particle Engineering, Graz University of Technology, Inffeldgasse 13, 8010 Graz, Austria. Tel.: +43 316 873 30400.
E-mail address: khinast@tugraz.at (J. Khinast).

http://dx.doi.org/10.1016/j.ces.2015.05.035
0009-2509/

(2005), who used FVM with an Eulerian multiphase method to simulate the flow in a partially filled twin-screw.

In Part 2 of this work, we present a detailed analysis of the extruder screw elements with regard to mixing. Numerical studies of mixing in extruders are mostly based on the tracking of tracer particles (e.g., Kalyon et al., 1988; Lawal et al., 1993; Lawal and Kalyon, 1995a, 1995b; Ishikawa, 2001; Rodríguez, 2009; Cleary and Robinson, 2011; Sarhangi Fard et al., 2012; Sarhangi Fard and Anderson, 2013). However, results obtained with tracer particles typically depend on the used initial configuration of the tracer, and a more general quantification of mixing would be desirable. Dispersion coefficients are tracer-independent quantities of the flow field and could be used to quantify dispersive mixing; however, their evaluation requires a rigorous distinction between convective and dispersive transport, which is a challenge for the complex flow in co-rotating twin-screws. Yang and Manas-Zloczower (1992) proposed a parameter termed "mixing index", which indicates the local type of flow on a scale between 0 and 1, where 0 indicates pure rotational flow, 0.5 pure shear flow and 1 pure elongational flow. This can be qualitatively correlated to the mixing and was used to study mixing in co-rotating twin-screw extruders (e.g., Yang and Manas-Zloczower, 1992; Zhu et al., 2013; Rathod and Kokini, 2013; Lawal et al., 1993; Lawal and Kalyon, 1995b). Similarly, the so-called finite-time Lyapunov exponents can be used for the quantification of the local stretching of fluid elements and for the detection of attracting and repelling manifolds, (e.g., Robinson et al., 2008; Robinson and Cleary, 2012). Although, these parameters are well suited to analyze the spatial distribution of the mixing, they do not allow the quantification of resulting product properties.

Since the achievement of certain product properties is usually the target in applications, we followed the mostly used approach and analyzed mixing based on tracer particles. Specifically, we evaluated the intensity of segregation on a grid of cubed cells and tracked its time evolution during several screw revolutions. Subsequently, we fitted exponential functions through these data in order to determine the mixing kinetics, which might be used to predict mixing in simplified models of extrusion processes (e.g., Eitzlmayr et al., 2013, 2014).

2. Evaluation of mixing

The current mixing study is based on the simulations presented in Part 1, which were conducted using the open-source particle simulator LIGGGHTS (Kloss et al., 2012). Since the SPH fluid elements represent Lagrangian particles, we employed them as tracer particles by marking them at a defined time. This was done after 0.5 revolutions, which was sufficient to obtain a developed flow. Initially, the tracer was a slice extending over a half of the cross-section and a third of the axial length (see Fig. 1, top). This configuration was chosen in order to indicate cross mixing and axial mixing in combination, as it also occurs in reality. Clearly, to describe the mixing of this tracer completely, requires tracking until a homegeneous mixture is achieved. However, this was not possible due to the computational expense. Thus, we conducted the simulations during five revolutions, which was sufficient to fit kinetic laws. Snapshots of tracer positions during the revolutions are illustrated in Fig. 1 for an exemplary case.

In order to quantify the mixing process, we used a grid of cubed cells (cell size 2 mm and volume 8 mm³, see Fig. 2 top) and calculated the amount of tracer particles in each cell and its standard deviation. To correctly evaluate the standard deviation, a constant sample size is required. This was unattainable due to inevitable variations in the particle count per cell (e.g., caused by density variations, cells being divided by the walls and not completely filled or due to particles located at the cell interfaces and being divided by the interfaces). The average particle count inside each cell was calculated from the entire volume of 132,617 mm³ and the total particle count of 981,278, yielding 59.2 per cell. To approximate a constant sample size, we did not consider cells with less than 57 and more than 61 particles and only used cells with a particle count between 57 and 61 (i.e., with a variation of the sample size of about ± 3%). As a result, approximately 50% of all particles were considered to calculate the standard deviation in the completely filled cases.

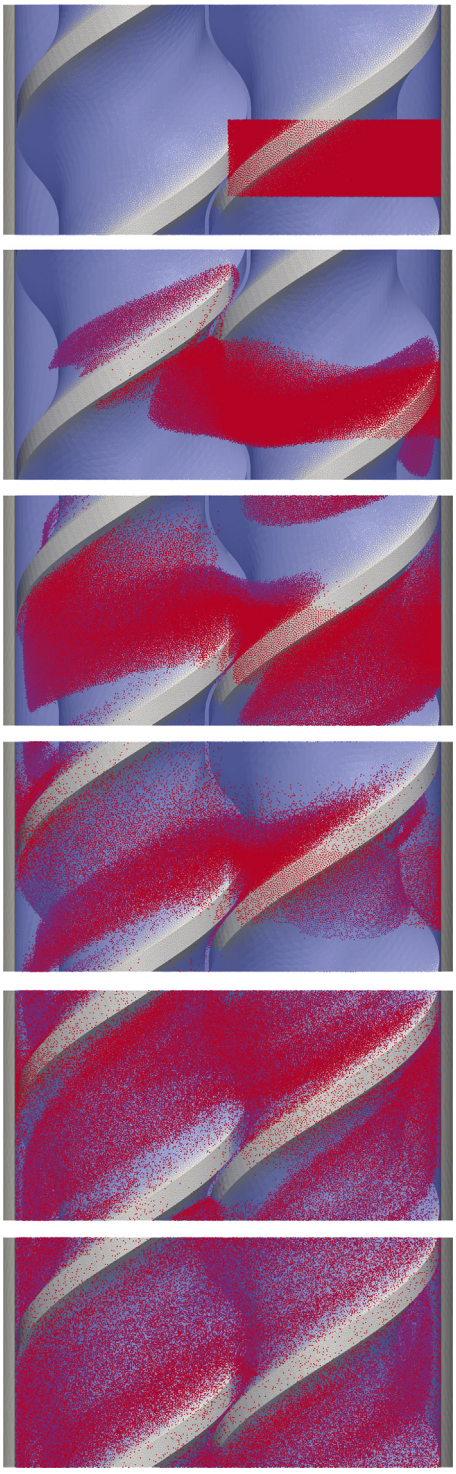

Fig. 1. Snapshots of the tracer particle positions for Scenario 1 ($a_z = 25$ m/s², corresponding to $\dot{V}/nD = 0.057$, see Part 1 for more details). The conveying direction was towards the top. The time from top to bottom: 0, 0.25, 0.5, 1, 2 and 4 revolutions.

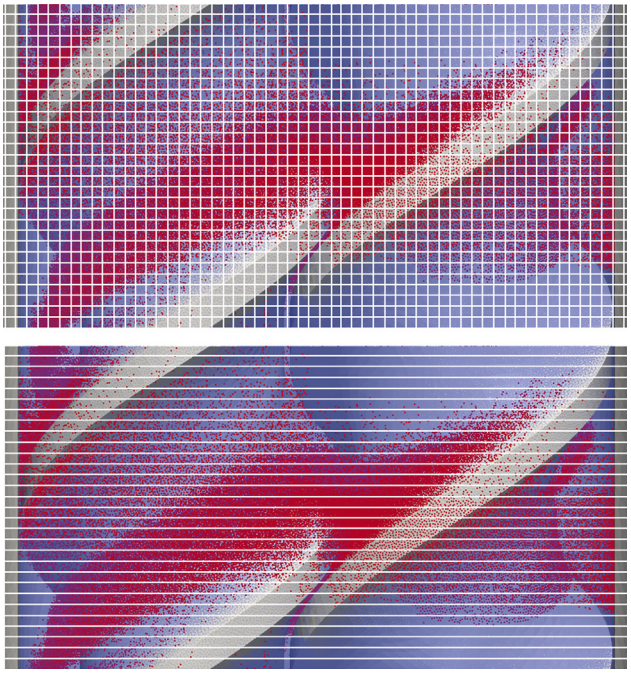

Fig. 2. Grids used for the mixing evaluation: cubed cells of 2 mm size (top), slices 2 mm thick (bottom).

We normalized the standard deviation σ of the tracer content to give the intensity of segregation S (where N_{tracer} is the number of tracer particles and N_{total} the total particle number):

$$S = \frac{\sigma}{\sqrt{\frac{N_{tracer}}{N_{total}} \cdot \left(1 - \frac{N_{tracer}}{N_{total}}\right)}} \tag{1}$$

Fig. 3 shows the time evolution of S for an exemplary case ($a_z = 10$ m/s²).

In order to consider axial mixing separately, we applied the same procedure to cross-sectional slices (2 mm thick, see Fig. 2 bottom) in the axial direction (i.e., one slice unified all cells in the same axial position). Since the cross sectional areas of the screws and barrel are constant in the axial direction and each slice contained the same amount of fluid volume, we considered all slices in this case. This yielded a similar time evolution of the segregation intensity S_{ax} (Fig. 3) but only starting at around 0.6 rather than 1 since initially the tracer did not extend over the entire cross section (i.e., the initial state was not fully segregated). In all cases, the time evolution of S_{ax} was less regular than that of S, possibly due to a lower number of samples (30 slices vs. about 8000 cubed cells).

For both S and S_{ax} a pronounced inflection point after almost one revolution can be observed. This is due to the limited axial extension of the domain and the periodic boundary conditions in the axial direction, i.e., when the convective flow in the axial direction transported the tracer once through the entire domain it was coarsely distributed and the axial convection did not further support mixing. This is also illustrated in Fig. 1: after 0.5 revolutions some of the tracer already crossed the periodic boundary and after 1 revolution the tracer was distributed along the axial direction. The further decrease in S_{ax} over time was obviously much slower than that during the first half revolution. The difference in the mixing rates was less pronounced for S since it involved not only axial but also cross mixing. A similar effect did not occur in the cross-sectional direction with no periodic boundaries to affect mixing in this case.

In order to determine mixing kinetics for the various mechanisms, we fitted exponential decay functions in each section of the

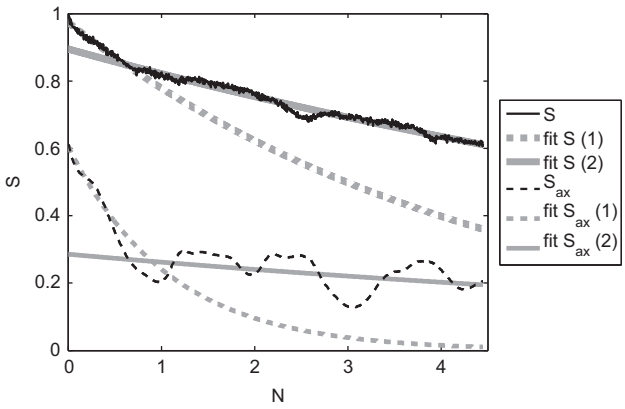

Fig. 3. Intensity of segregation versus the number of revolutions evaluated through cubed cells (S) and cross-sectional slices (S_{ax}).

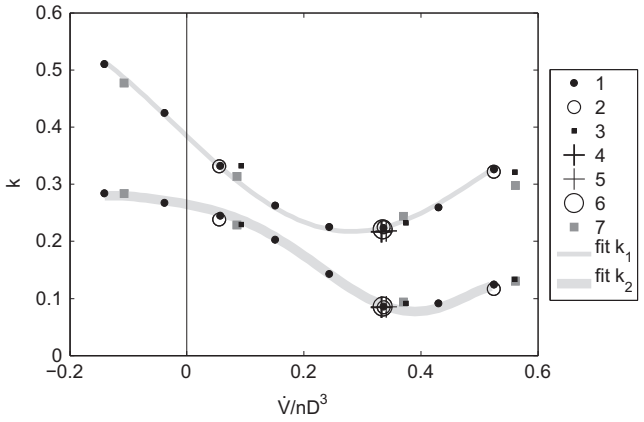

Fig. 4. Mixing rates k_1 and k_2 (determined on cubed cells) versus the dimensionless flow rate in the completely filled state.

determined evolutions curves (Fig. 3):

$$S = S_0 e^{-kN} \tag{2}$$

$$S_{ax} = S_{ax,0} e^{-k_{ax} N} \tag{3}$$

3. Results and discussion

The resulting values for the mixing rates before (k_1 and $k_{ax,1}$) and after (k_2 and $k_{ax,2}$) the inflection point are shown in Figs. 4 and 5 versus the dimensionless flow rate for the completely filled simulations (Scenarios 1–7). For the partially filled simulations (Scenario 8), the analogous mixing rates are shown in Figs. 6 and 7 versus the normalized flow rate Λ. For a detailed presentation of Scenarios 1–8 see Part 1.

Mixing variations due to different simulation parameters for Scenarios 1–7 were insignificant and almost no systematic difference was observed. Moreover, the mixing phenomena were well reproduced by the coarser resolution of 1 mm without the clearance flow (Scenario 7), which required much less computational expense compared to the resolution of 0.5 mm.

In the partially filled state (Scenario 8), for filling ratios below $f = 0.75$ the first phase and the inflection point could not be identified due to increasing irregularities in the time evolution of S with decreasing filling ratio. This is possibly due to an insufficiently low number of sample cells since at low filling ratios most cells were only partially filled in the partially filled screw element and not considered when evaluating S. Thus, data points for k_1 are not shown below

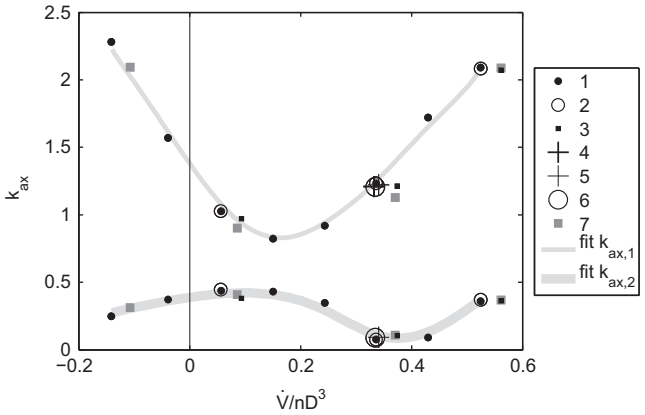

Fig. 5. Mixing rates $k_{ax,1}$ and $k_{ax,2}$ (determined on the cross-sectional slices) versus the dimensionless flow rate in the completely filled state.

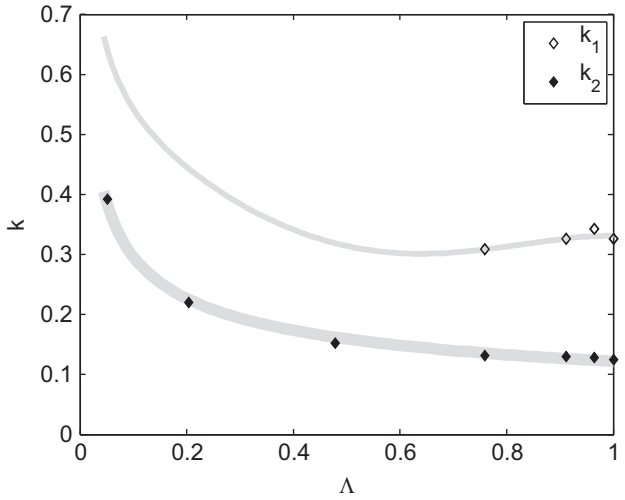

Fig. 6. Mixing rates k_1 and k_2 (determined on cubed cells) versus the normalized flow rate Λ in the partially filled state.

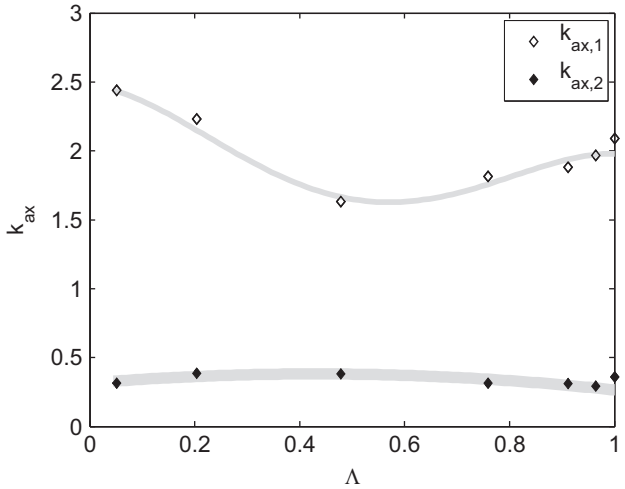

Fig. 7. Mixing rates $k_{ax,1}$ and $k_{ax,2}$ (determined on the cross-sectional slices) versus the normalized flow rate Λ in the partially filled state.

$f=0.75$ (corresponding to $\Lambda \approx 0.75$) in Fig. 6. The reason why we showed a fit for the missing k_1 data is explained below. This was not the case for the axial mixing rate k_{ax} (see Fig. 7) since we took all cross-sectional slices into account (assuming that the fluid was uniformly distributed along the axial direction).

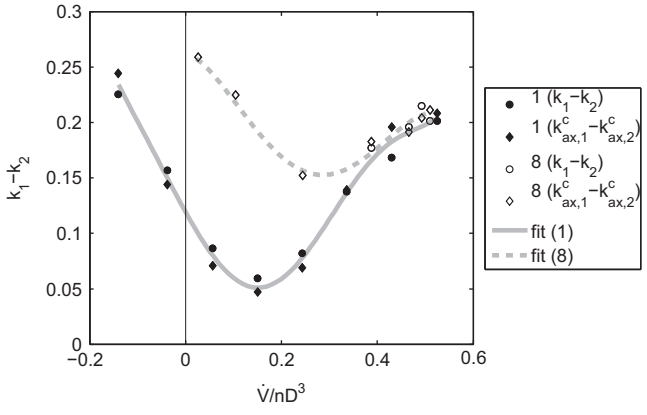

Fig. 8. Mixing rates k_1-k_2 and $k^c_{ax,1}-k^c_{ax,2}$ versus the dimensionless flow rate in the completely filled state (Scenario 1) and the partially filled state (Scenario 8).

Clearly, the mixing rates k and k_{ax} are quantitatively not comparable since the considered sample sizes for S and S_{ax} varied significantly (i.e., each cubed cell contained the average particle number of 59 and the cross-sectional slices about 32,000 at $f=1$). However, the differences k_1-k_2 and $k_{ax,1}-k_{ax,2}$ versus the flow rate yielded qualitatively similar curves, which supported the above suggestion that these differences occurred for the same reason, i.e., due to axial convection. Fig. 8 shows both curves for the completely filled state (Scenario 1) and the partially filled state (Scenario 8), where we adjusted the axial mixing rates k_{ax} by a linear factor in order to collapse the curves. The adjusted axial mixing rates were named k^c_{ax}:

$$k^c_{ax} = \frac{k_{ax}}{\kappa} \tag{4}$$

The conversion factor κ, which was determined from the average of the k and k_{ax} values, was 8.32 and 8.20 in the completely and partially filled states, respectively. We fitted polynomials using the data shown in Fig. 8. Clearly, the curves in the completely and partially filled cases converged with the vanishing pressure drop and as the filling ratio approached one (i.e., inherent conveying). Based on that, we developed the fits for k_1, k_2, $k_{ax,1}$ and $k_{ax,2}$ shown in Figs. 4–7, i.e., one curve of k_1 and k_2 was fitted and the other was calculated based on the fits for k_1-k_2 and $k_{ax,1}-k_{ax,2}$ (for mathematical functions see the Appendix). This is why the fit of k_1 for the partially filled state (Fig. 6) is shown in the region $\Lambda < 0.75$ where no data points were available (i.e., k_2 was fitted and k_1 obtained from the fits of k_2 and k_1-k_2).

Fig. 9 shows how different effects contributed to overall mixing. For a more compact representation, the resulting fits for the completely and partially filled states are shown together, specifically the overall mixing rates k_1 and k_2 and the difference $k_2-k^c_{ax,2}$. The top curves for both states represent k_1, which is the overall mixing rate that includes all mixing mechanisms. The middle curves show k_2, which is similar to k_1 but without mixing via axial convection and thus, reflects cross mixing and axial dispersion. Similarly, $k_{ax,1}$ includes both axial mixing mechanisms, i.e., axial convection and axial dispersion. Since the difference between $k_{ax,1}$ and $k_{ax,2}$ is axial convection, $k_{ax,2}$ reflects axial dispersion. The difference $k_2-k^c_{ax,2}$ represented by the lower curves in Fig. 9 can be interpreted as the effect of cross mixing, which could not be further analyzed based on these data.

For practical considerations, the mixing rate k_2 is the most relevant one (i.e., the thick lines in Fig. 9) since extruders are typically used for mixing continuous material streams, where the effect of axial convection on mixing vanishes in the same manner as it does in our simulations (after the inflection point in the evolutions of S and S_{ax}).

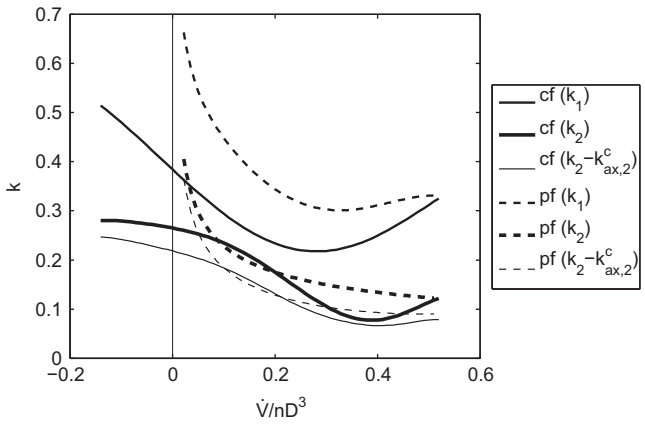

Fig. 9. Fitted curves for the mixing rates k_1, k_2 and k_2–$k^c_{ax,2}$ versus the dimensionless flow rate in the completely filled state "cf" (Scenario 1) and the partially filled state "pf" (Scenario 8).

In the completely filled state, the mixing rate k_2 was the lowest at $\dot{V}/nD^3 \approx 0.4$ (i.e., about 75% of the inherent conveying capacity), which was caused by low axial dispersion and reduced cross mixing. Axial dispersion obviously collapsed since the axial velocity in the screw channels decreased due to backpressure and became more uniform compared to conveying without backpressure (see the results presented in Part 1). The respective flow rate $\dot{V}/nD^3 \approx 0.4$ is of less practical significance since extruders are typically operated in the range of $\dot{V}/nD^3 < 0.2$ (in pharmaceutical applications mostly < 0.1).

With the increasing backpressure and the decreasing flow rate, cross mixing and axial dispersion increased and reached maximum values in the region of negative flow rates (i.e., backward conveying elements). The reason could be increased backflow along the channels with increased backpressure, which affects both axial and cross mixing since the trajectories along the channels were extended in both, the axial and the cross directions. Interestingly, axial dispersion was the highest at $\dot{V}/nD^3 \approx 0.1$ and decreased slightly at flow rates around and below zero (see $k_{ax,2}$ in Fig. 5).

However, the rate of axial convection mixing (i.e., the difference k_1–k_2) was the lowest at $\dot{V}/nD^3 \approx 0.15$, which corresponds to zero flow rates in the screw channels (as presented in Part 1). Axial convection increased mixing significantly with increasing flow rate in the screw channels. The corresponding curves for complete and partial filling converged during inherent conveying (neglecting fitting inaccuracies), i.e., during changeover of the complete and partial fillings at $\dot{V}/nD^3 \approx 0.52$. As the filling ratio and the flow rate decreased, the mixing rates in the partially filled screw element mainly increased (except a slight decrease in mixing via axial convection) due to the increased cross mixing. In contrast, axial dispersion remained nearly constant over the entire range of the filling ratios and flow rates (see $k_{ax,2}$ in Fig. 7). The increase in cross mixing with the decreasing filling ratio can be explained by the increase in the relative amount of material flowing through the clearances in the circumferential direction. This dramatically enhances cross mixing below $f=0.1$. The effect of axial convection on mixing (see Fig. 8) varied less depending on the flow rate in the partially filled state than in the completely filled state, possibly due to the absence of backflow in the partially filled state. The minimum axial convection mixing rate $k_{ax,1}$–$k_{ax,2}$ occurred at approximately 50% of the inherent conveying capacity (i.e., $f \approx 0.5$), however, this has fewer practical implications since axial convection is of minor significance for applications.

Interestingly, the mixing rates in the partially filled state were mostly higher than those in the completely filled state (see Fig. 9), especially at low filling ratios $f < 0.1$. However, note that the mixing rates k and k_{ax} are defined as a relative change in the intensity of segregation per screw revolution, as the derivative of Eq. (2) implies (the same applies for Eq. (3)):

$$k = -\frac{1}{S}\frac{dS}{dN} \tag{5}$$

Thus, the effect of residence time was not incorporated into the mixing rates k and k_{ax}, although this constitutes an important difference for the completely and partially filled screw sections. To demonstrate the effect residence time, we estimated the mixing effect versus the flow rate in the completely and partially filled screw sections for a given length of the screw section. Based on the length L, the free cross section area A_{cr}, the filling ratio f and the flow rate $\dot{V}$ the average residence time τ can be estimated as

$$\tau = \frac{f A_{cr} L}{\dot{V}} \tag{6}$$

Together with the screw speed n, the number of screw revolutions during time τ is $N = n\tau$. Substituting this in Eq. (2) for an initially unmixed state ($S_0 = 1$) yields

$$S = \exp\left(-\frac{k\, n\, f\, A_{cr}\, L}{\dot{V}}\right) \tag{7}$$

Clearly, this is only an estimate since it fails to account for the distribution of residence time. However, it includes the main influences and reflects at least qualitative trends. Based on Eq. (7), we estimated S for the completely filled and partially screw sections using the fits for the practically relevant mixing rate k_2 (as show in Fig. 9).

The results are shown in Fig. 10 versus the flow rate for various length-to-diameter ratios L/D of the considered screw section. In contrast to the results for the mixing rates, due to longer residence time mixing is more effective in the completely filled screw sections than in the partially filled screw sections. In all cases, the best mixing occurs at flow rates around zero due to an increase in the residence time caused by a decrease in the flow rate. At flow rates of almost zero the intensity of segregation for the partially filled screw sections converged to zero, i.e., at filling ratios close to zero suitable mixing occurred even in the partially filled screw section due to a high relative amount of the clearance flow. Similar trends were described in experimental results for a single-screw extruder (Pawlowski, 1971; Kohlgrüber, 2008).

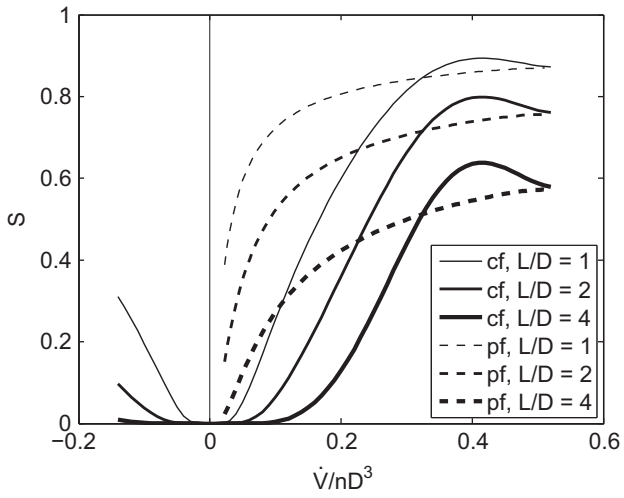

Fig. 10. Intensity of segregation S versus the dimensionless flow rate determined from the fit for the mixing rate k_2 in a screw section with a given length-to-diameter ratio L/D (cf – completely filled, pf – partially filled).

These trends suggest that the lowest possible dimensionless flow rates result in good mixing. However, besides higher investment costs that are required to achieve a lower flow rate for a given production rate in larger extruders, the specific mechanical energy consumption (SMEC, i.e., the energy required to rotate the screws in kWh per kg material) increases significantly as the residence time and the mixing performance increase. This is illustrated in Fig. 11 which shows the ratio between the dimensionless driving power and the dimensionless flow rate (yielding the SMEC in dimensionless form, $PD/\dot{V}\eta nL$) versus the flow rate for Scenarios 1 and 8 for the complete and partial fillings, respectively. With the decreasing flow rate, i.e., with the increasing residence time, the SMEC increased dramatically. However, in the practically relevant operation range of $\dot{V}/nD^3 < 0.1$–0.2, the specific energy consumption was always much lower for the partial filling than for the complete one, which indicates that a partially filled section is suitable for the thermal relaxation of a material after a completely filled mixing zone. Clearly, mixing of highly-viscous materials requires energy. The better the mixing performance, the higher the SMEC, as Figs. 10 and 11 show. In practical applications, to avoid excessive energy input and stress to the material (especially in the pharmaceutical manufacturing that typically involves sensitive materials), it is very important to design the processes in such a way that residence time and mixing are sufficient but not overstated.

4. Summary and conclusions

In this study, we present a detailed investigation of the mixing phenomena in a conveying element of a co-rotating twin-screw extruder in completely and partially filled states based on the SPH simulations presented in Part 1. We tracked tracer particles during several revolutions and evaluated the time evolution of the intensity of segregation using two different grids, indicating overall mixing and pure axial mixing. Based on that, we fitted kinetic laws and analyzed the contributions of axial and cross mixing to the overall mixing rate in various operation states.

Finally, we showed the importance of residence time along with the mixing rates per screw revolution: due to a higher residence time, the mixing performance was higher in the completely filled screw sections than in the partially filled screw sections, and the mixing performance increased with the decreasing flow rate. However, better mixing due to a higher residence time led to an increased specific mechanical energy consumption, meaning that in practice it is essential to find a compromise between good mixing and low energy input, especially with regard to sensitive materials.

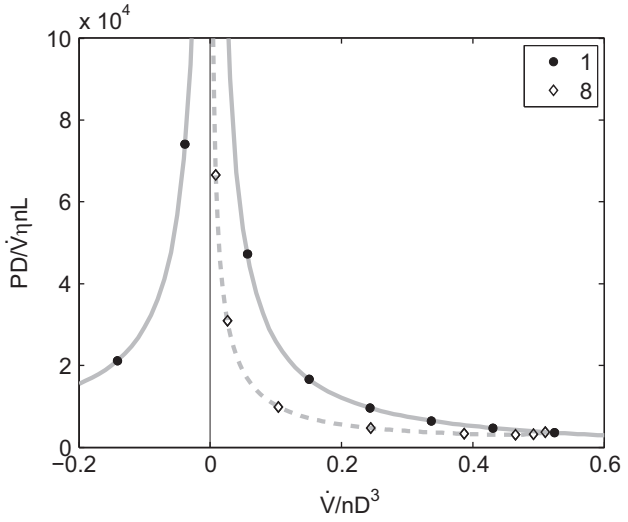

Fig. 11. Specific mechanical energy consumption (SMEC) in the dimensionless form over the dimensionless flow rate for Scenario 1 (completely filled) and Scenario 8 (partially filled).

This work also underlines the potential of the SPH method for the simulation of flow and mixing in co-rotating twin-screw extruders and demonstrates that results in excellent agreement with CFD data from the literature can be achieved. Thus, the presented approach is a robust tool for further investigations of flow and mixing in other screw element geometries. Clearly, the studied conveying element is only one type of screw elements among a variety of different geometries available for practical applications, e.g., conveying elements with various pitch-to-diameter ratios, kneading elements with different disc sizes and stagger angles, and specific mixing elements. This will be reported in future communications.

Furthermore, our work provides a basis for refining empirical models of completely and partially filled screw elements. Our results may lead to an improvement of (more time-efficient) one-dimensional (1D) simulation tools for numerical studies of the entire extrusion process, facilitating the design, optimization and scale-up of extrusion processes.

Notation

Latin symbols

A_{cr}	free cross section area [m²]
a_z	mass specific body force in the z direction [m/s²]
D	barrel diameter [m]
f	filling ratio [dimensionless]
k	mixing rate, related to S [dimensionless]
k_{ax}	mixing rate, related to S_{ax} [dimensionless]
k_{ax}^c	mixing rate k_{ax}, converted by the factor κ [dimensionless]
L	length [m]
N	number of revolutions [dimensionless]
n	screw speed [s^{-1}]
P	power [W]
S	intensity of segregation, indicating overall mixing [dimensionless]
S_{ax}	intensity of segregation, indicating pure axial mixing [dimensionless]
$\dot{V}$	flow rate [m³/s]

Greek symbols

η	dynamic viscosity [Pa s]
κ	conversion factor for the mixing rates [dimensionless]
Λ	normalized flow rate [dimensionless]
σ	standard deviation of the tracer content [dimensionless]
τ	mean residence time [s]

Acknowledgments

This work was funded through the Austrian COMET Program by the Austrian Federal Ministry of Transport, Innovation and Technology (BMVIT), the Austrian Federal Ministry of Economy, Family and Youth (BMWFJ) and by the State of Styria (Styrian Funding Agency SFG). The authors would like to thank NAWI Graz for providing access to the high performance computing system dcluster.tugraz.at. Special thanks go to Stefan Radl (Graz University of Technology, Institute for Process and Particle Engineering) for assistance with the LIGGGHTS code and

to Christoph Kloss (DCS Computing GmbH) for assistance with processing of STL-meshes in LIGGGHTS.

References

Bierdel, M., 2008. Computational fluid dynamics. In: Kohlgrüber, K. (Ed.), Co-Rotating Twin-Screw Extruders. Carl Hanser Publishers, Munich.

Breitenbach, J., 2002. Melt extrusion: from process to drug delivery technology. Eur. J. Pharm. Biopharm. 54, 107–117.

Cleary, P.W., Robinson, M., 2011. Understanding viscous fluid transport and mixing in a twin screw extruder. In: 8th International Conference on CFD in Oil & Gas, Metallurgical and Process Industries. Trondheim, Norway.

Douroumis, D., 2012. Hot-melt Extrusion: Pharmaceutical Applications. John Wiley & Sons, Ltd., Chichester.

Eitzlmayr, A., Khinast, J., 2015. Co-rotating twin-screw extruders: detailed analysis of conveying elements based on smoothed particle hydrodynamics. Part 1: Hydrodynamics. Chem. Eng. Sci. http://dx.doi.org/10.1016/j.ces.2015.04.055 (online).

Eitzlmayr, A., Khinast, J., Hörl, G., Koscher, G., Reynolds, G., Huang, Z., Booth, J., Shering, P., 2013. Experimental characterization and modeling of twin-screw extruder elements for pharmaceutical hot melt extrusion. AIChE J. 59, 4440–4450.

Eitzlmayr, A., Koscher, G., Reynolds, G., Huang, Z., Booth, J., Shering, P., Khinast, J., 2014. Mechanistic modeling of modular co-rotating twin-screw extruders. Int. J. Pharm. 474, 157–176.

Ghebre-Sellassie, I., Martin, C., 2003. Pharmaceutical Extrusion Technology. Marcel Dekker Inc., New York.

Ishikawa, T., 2001. 3-D non-isothermal flow field analysis and mixing performance evaluation of kneading blocks in a co-rotating twin srew extruder. Polym. Eng. Sci. 41, 840–849.

Kalyon, D.M., Gotsis, A.D., Yilmazer, U., Gogos, C.G., Sangani, H., Aral, B., Tsenoglou, C., 1988. Development of experimental techniques and simulation methods to analyze mixing in co-rotating twin screw extrusion. Adv. Polym. Technol. 8, 337–353.

Kleinebudde, P., 2011. Pharmazeutisches Produktdesign: Gezielte Freisetzung von Wirkstoffen durch unterschiedliche Extrusionstechniken. Chemie Ing. Tech 83, 589–597.

Kloss, C., Goniva, C., Hager, A., Amberger, S., Pirker, S., 2012. Models, algorithms and validation for opensource DEM and CFD-DEM. Prog. Comput. Fluid Dyn. Int. J. 12, 140–152.

Kohlgrüber, K., 2008. Co-Rotating Twin-Screw Extruders. Carl Hanser Publishers, Munich.

Lawal, A., Kalyon, D.M., 1995a. Simulation of intensity of segregation distributions using three-dimensional FEM analysis: application to corotating twin screw extrusion processing. J. Appl. Polym. Sci. 58, 1501–1507.

Lawal, A., Kalyon, D.M., 1995b. Mechanisms of mixing in single and co-rotating twin screw extruders. Polym. Eng. Sci. 35, 1325–1338. http://dx.doi.org/10.1002/pen.760351702.

Lawal, A., Kalyon, D.M., Ji, Z., 1993. Computational study of chaotic mixing in co-rotating two-tipped kneading paddles: two-dimensional approach. Polym. Eng. Sci. 33, 140–148. http://dx.doi.org/10.1002/pen.760330304.

Monaghan, J.J., 1994. Simulating free surface flows with SPH. J. Comput. Phys. 110, 339–406.

Monaghan, J.J., 2000. SPH without a tensile instability. J. Comput. Phys. 159, 290–311. http://dx.doi.org/10.1006/jcph.2000.6439.

Monaghan, J.J., 2005. Smoothed particle hydrodynamics. Rep. Prog. Phys. 68, 1703–1759. http://dx.doi.org/10.1088/0034-4885/68/8/R01.

Pawlowski, J., 1971. Die Ähnlichkeitstheorie in der physikalisch-technischen Forschung. Springer Publishers, Berlin/Heidelberg, Germany.

Pokriefke, G., 2005. Numerische Analyse reibungsbehafteter Strömungen in teilgefüllten Extrudern. Universität der Bundeswehr, Hamburg.

Rathod, M.L., Kokini, J.L., 2013. Effect of mixer geometry and operating conditions on mixing efficiency of a non-Newtonian fluid in a twin screw mixer. J. Food Eng. 118, 256–265.

Repka, M.A., Langley, N., DiNunzio, J., 2013. Melt Extrusion – Materials, Technology and Drug Product Design. Springer, New York, Heidelberg, Dordrecht, London http://dx.doi.org/10.1007/978-1-4614-8432-5.

Robinson, M., Cleary, P., Monaghan, J., 2008. Analysis of mixing in a twin cam mixer using smoothed particle hydrodynamics. AIChE J. 54, 1987–1998. http://dx.doi.org/10.1002/aic.

Robinson, M., Cleary, P.W., 2012. Flow and mixing performance in helical ribbon mixers. Chem. Eng. Sci. 84, 382–398. http://dx.doi.org/10.1016/j.ces.2012.08.044.

Rodríguez, E.O., 2009. Numerical Simulations of Reactive Extrusion in Twin Screw Extruders. Waterloo, Canada.

Sarhangi Fard, A., Anderson, P.D., 2013. Simulation of distributive mixing inside mixing elements of co-rotating twin-screw extruders. Comput. Fluids 87, 79–91.

Sarhangi Fard, A., Hulsen, M.A., Meijer, H.E.H., Famili, N.M.H., Anderson, P.D., 2012. Tools to simulate distributive mixing in twin-screw extruders. macromol. Theory Simul. 21, 217–240.

Yang, H.-H., Manas-Zloczower, I., 1992. Flow field analysis of the kneading disc region in a co-rotating twin screw extruder. Polym. Eng. Sci. 32, 1411–1417.

Zhu, X.Z., Wang, G., He, Y.D., 2013. Numerical simulation of temperature and mixing performances of tri-screw extruders with non-isothermal modeling. Res. J. Appl. Sci. Eng. Technol. 5, 3393–3401.